

# The Effects of Torsion on Anomalous Diffusion in Helical Pipe

Flow

by

Michael B. Gratton

Andrew J. Bernoff, Advisor

Advisor: \_\_\_\_\_

Second Reader: \_\_\_\_\_

(Anette E. Hosoi)

May 2002

Department of Mathematics

**HARVEY MUDD**  
**COLLEGE**

## Abstract

# The Effects of Torsion on Anomalous Diffusion in Helical Pipe Flow

by Michael B. Gratton

May 2002

This thesis investigates the advection and diffusion of a passive scalar in helical pipes. By assuming that the curvature and torsion are small (equivalent to small Dean number) and the Reynolds number is moderate, we derive a closed form approximation for the induced recirculating flow. We find a stream function for the Poincaré map between cross sections that depends only on the geometric parameter  $\lambda$ , a rescaled ratio of torsion to curvature. Using a simple numerical scheme, we simulate advection-diffusion by composing this map with random-walk diffusion. We discover four mixing time scales, including two “anomalous” mixing time scales, where the width of the distribution of the mixing scalar is proportional to  $t$  (as postulated by Mezic & Wiggins (1994)), rather than  $\sqrt{t}$ . The effect of  $\lambda$  on the mixing is studied, and scaling laws for each regime are developed.

# Table of Contents

<b>List of Figures</b>	<b>iii</b>
<b>Chapter 1: Introduction</b>	<b>1</b>
1.1 Plan of the thesis . . . . .	2
1.2 A basic introduction to diffusion and advection . . . . .	2
1.3 Taylor diffusion . . . . .	4
<b>Chapter 2: Derivation of toroidal and helical flow fields</b>	<b>6</b>
2.1 A general pipe coordinate system . . . . .	6
2.2 Torodial pipe flow equations . . . . .	8
2.3 Helical pipe flow equations . . . . .	12
<b>Chapter 3: Stream functions for toroidal and helical pipe flow fields</b>	<b>14</b>
3.1 A method for creating stream functions . . . . .	14
3.2 Deriving the stream functions . . . . .	15
3.3 Consequences of the helical stream function . . . . .	20
<b>Chapter 4: Numerical methods</b>	<b>21</b>
4.1 Simulating advection . . . . .	22
4.2 Simulating diffusion . . . . .	23
4.3 Composing advection and diffusion: error analysis . . . . .	26
4.4 Flow visualization . . . . .	28

<b>Chapter 5: The effects of torsion on mixing</b>	<b>33</b>
5.1 The four mixing regimes . . . . .	33
5.2 Non $\lambda$ -dependent mixing regimes . . . . .	35
5.3 $\lambda$ -dependent anomalous mixing . . . . .	36
5.4 Taylor Dispersion dependence on torsion . . . . .	39
<b>Chapter 6: Conclusion</b>	<b>40</b>
6.1 Results . . . . .	40
6.2 Future work . . . . .	41
<b>Bibliography</b>	<b>42</b>

## List of Figures

2.1	Cross-sectionally defined coordinates . . . . .	7
3.1	Streamlines for toroidal velocity field . . . . .	16
3.2	Poincaré map streamlines for a helical pipe . . . . .	19
4.1	Particle/boundary interactions . . . . .	26
4.2	Mixing visualization: $\lambda = 0$ . . . . .	29
4.3	Mixing visualization: $\lambda = 0.1$ . . . . .	30
4.4	Mixing visualization: $\lambda = 1$ . . . . .	31
4.5	Mixing visualization: advection and diffusion together . . . . .	32
5.1	A Plot of $\sigma$ versus $t$ . . . . .	34
5.2	$\sigma$ versus $t$ for various values of $\lambda$ . . . . .	37
5.3	The transition time $t_t$ dependence on $\lambda$ . . . . .	38
5.4	Anomalous II regime slope $m_\lambda$ versus $\lambda$ . . . . .	38
5.5	The Taylor Diffusion constant's dependence on $\lambda$ . . . . .	39

## Acknowledgments

I am indebted to Andrew J. Bernoff for his patience and insight on this project, and also to Crystal Williams for another kind of patience and for putting up with me during the hectic final stages.

# Chapter 1

## Introduction

We consider a rigid pipe with a circular cross-section of constant radius. The pipe is full of fluid being forced through it by a constant pressure gradient, and the fluid inside of the pipe flows with a local velocity depending on the bends and twists of the pipe, due to viscous drag along the walls of the pipe and centripetal forces caused by bends. This thesis considers helical pipes (with constant curvature and torsion), as well as the degenerate cases of toroidal pipes (constant curvature and no torsion) and straight pipes (no curvature or torsion). Note that curvature and torsion here refer to the properties of the centerline of the pipe. We want to model the fluid motion for various values of curvature and torsion in order to study the effects of the geometry on the velocity field and the fluid mixing inside the pipe.

For this problem, we will use a passive scalar  $H(x, y, s, t)$ , a scalar valued function that is deformed by the fluid flow. A passive scalar is an idealization of the physical problem of dye mixing in water: even very high concentrations (large values of  $H$ ) result in no change to the fluid behavior at that point; the scalar has no mass, requires no momentum to move it about – in every respect it is simply a place-marker. We control the initial position of the scalar (initial conditions on  $H$ ) and we want to measure its shape at a later time. The degree of mixing of  $H$  is measured via the standard deviation of  $H$ . This will be defined later rigorously in terms of the moments of  $H$ , but for now it

is enough to know that this is the “shoulder to shoulder width” of a plot of  $H$  with respect to one of its spatial variables. For example, the mixing along the  $z$ -axis would be characterized by  $\sigma_z(t)$ . Plots of  $\sigma_z$  versus time might display various mixing regimes where  $\sigma_z$  grows with different powers of  $t$ . Note that all other spacial dimensions are averaged out by this definition of mixing.

### **1.1 Plan of the thesis**

This chapter will develop the basic forces which act in mixing providing a basic introduction to the concepts covered in depth later: advection, diffusion, and Taylor diffusion (following Taylor’s more simplistic derivation [10]). Chapter 2 develops flow equations for the toroidal and helical pipe geometries following the work of Dean [2], Ward-Smith [11], and Germano [3] [4]. This analysis is complemented in Chapter 3 by the derivation of a general stream function for the Poincaré map between helical pipe cross-sections. Using this map and a random-walk simulation of diffusion, Chapter 4 outlines a particle-based numerical mixing simulation, analyzes the dependence of the numerical error on the system parameters, and provides a gallery of pictures displaying the effect of geometry on the fluid mixing. This simulation leads us to the description of the effects of torsion on the mixing in Chapter 5, specifically, the dependence of mixing regimes on pipe geometry. We also develop a method for averaging particles on streamlines that is useful for calculating  $\sigma$  in the limit of small diffusion or small timescales. Finally, Chapter 6 summarizes the major findings of the thesis and provides suggestions for future work in this area.

### **1.2 A basic introduction to diffusion and advection**

Two important factors influence mixing: diffusion and advection. Diffusion is the tendency of high concentrations of a substance to spread into neighboring

regions. If we consider heat, the heat diffuses so as to make hot spots cooler and nearby cool spots warmer. This is governed by the diffusion equation,

$$H_t = D\nabla^2 H, \tag{1.1}$$

where  $H = H(x, y, z, t)$  represents the concentration of some scalar (heat, dye, etc.) at a point in space and time. Note that we are using the subscript  $t$  to denote a partial derivative in time. This equation is generally useful in describing any diffusive effect. Note that this equation is in the Eulerian frame, i.e. the frame of an observer in the lab watching dye diffuse in water. Qualitatively, peaks of high concentration are eroded down to hills over time. A more physical explanation for this can be seen in the Lagrangian, or particle, frame. From this perspective, each molecule of dye or blob of heat experiences random collisions. These collisions are more frequent when there are more particles nearby, so areas of high concentration tend to spread apart. Diffusion, as considered in this problem, is a small but important effect. The scale of  $D$  is typically less than  $10^{-4}$ , while many of the other length scales in the problem considered are on the order of unity.

In addition to movement due to random collisions, particles also experience forces due to the fluid flow in the pipe. This problem assumes that the flow in the pipe is steady, incompressible, and irrotational. Essentially, the fluid in the pipe is non-turbulent and moving fairly slowly. In the Eulerian frame, we can state this as the basic advection equation,

$$H_t + \vec{u} \cdot \nabla H = 0, \tag{1.2}$$

which moves  $H = H(x, y, z, t)$  about the pipe with a velocity given by  $\vec{u} = \vec{u}(x, y, z)$ . Here  $\vec{u}$  does not depend on  $t$  because the flow was assumed to be steady. Determining  $\vec{u}$  depends on the geometry of the pipe.

### 1.3 Taylor diffusion

In pipe-flow mixing problems, the famous result of Taylor [10] provides great insight into the long-term mixing behavior. Taylor discovered that for  $t \gg 1/D$  and  $D$  is small, the concentration  $H$  spreads self-similarly about a point moving at the average velocity down the pipe. This self-similar spread results in

$$\sigma = \sqrt{2D_{eff}t}, \quad (1.3)$$

where  $\sigma$  is the standard deviation width of the passive scalar along the axis of the pipe,  $D_{eff} \approx k/D$ , and  $k$  is determined by the pipe geometry. We will follow Taylor's heuristic derivation of this result. Jones and Young provide a more mathematically complete result [12]. We consider a straight pipe with a circular cross-section of constant radius, and impose a no-slip boundary condition on the walls. The steady, incompressible flow of fluid is governed by pipe Bizek flow, giving rise to the the advection-diffusion equation

$$H_t + u_0(1 - \tilde{r}^2/a^2)\hat{z} \cdot \nabla H = D\nabla^2 H, \quad (1.4)$$

which is the combination of (1.1) and (1.2). Note that the velocity field is the result of viscous drag along the walls slowing fluid at the pipe walls to a standstill, while fluid at the centerline moves with the maximum speed,  $u_0$ . If we consider the problem in the obvious choice of cylindrical coordinates, it is natural to rescale all lengths by the pipe radius:  $r = \tilde{r}/a$ . If we assume that  $D$  is small compared to  $u_0$ , then movement of concentration  $H$  in the  $z$ -direction due to the diffusive term can be neglected:

$$H_t + u_0(1 - r^2)H_z = \frac{D}{a^2}(H_{rr} + \frac{1}{r}H_r). \quad (1.5)$$

Since the velocity field is simple, we consider changing frames to take advantage of self-similar behavior. Let  $\tilde{z} = z - \frac{1}{2}u_0t$ . This yields

$$\frac{a^2}{D}H_t + \frac{a^2u_0}{D}(\frac{1}{2} - r^2)H_{\tilde{z}} = H_{rr} + \frac{1}{r}H_r. \quad (1.6)$$

We can solve the above in the case where advection is a slower phenomena than the averaging of radial variations due to diffusion. In this case,  $H_t$  is approximately 0 and  $H_r$  is practically independent of  $z$ . Using the no-slip boundary conditions, we have

$$H = \hat{H} + \frac{a^2 u_0}{8D} H_{\tilde{z}} (r^2 - \frac{1}{2} r^4), \quad (1.7)$$

where  $\hat{H}$  is  $H$  evaluated at  $r = 0$ . The flux across a cross-section at any  $\tilde{z}$  can be written as

$$Q = -2\pi a^2 \int_0^1 u_0 (\frac{1}{2} - r^2) H r \, dr. \quad (1.8)$$

Another consequence of the assumption that transport is slow compared to cross-sectional diffusion is that the mean concentration in a cross-section,  $\bar{H}_{\tilde{z}}(\tilde{z})$ , is approximately the same as  $\hat{H}_{\tilde{z}}$ . Using  $H$  from (1.7) and the above expression for  $Q$ , we find

$$Q = -\frac{\pi a^4 u_0^2}{192D} \hat{H}_{\tilde{z}}. \quad (1.9)$$

If we let

$$D_{eff} = \frac{a^2 u_0^2}{192D}, \quad (1.10)$$

and use the fact that no fluid escapes during the flow of  $\bar{H}$ , we have the fluid continuity expression:

$$Q_{\tilde{z}} = -\pi a^2 \bar{H}_t, \quad (1.11)$$

or, combined with the above:

$$D_{eff} \bar{H}_{\tilde{z}\tilde{z}} = \bar{H}_t. \quad (1.12)$$

Notice that this is simply a one dimensional diffusion equation for the cross-sectionally averaged concentration  $\bar{H}$ . The assumptions made on the relative time scales of advection in  $z$  versus diffusion in  $r$  imply that this result is valid when  $H$  is well-diffused across the streamlines of the advective velocity  $u$ , i.e., when  $t \gg 1/D$ .

## Chapter 2

### Derivation of toroidal and helical flow fields

The geometry of the pipe determines the velocity field found inside. In this section, we investigate the helical geometry by building upon well-known results for the straight pipe and the toroidal pipe. The first task, developing a general coordinate system for any pipe geometry is undertaken in Section 2.1 by using a cross-sectional defined system. The straight-pipe equations are presented and analyzed. In Section 2.2, we follow Dean's [2] famous derivation of the toroidal pipe flow field. Then, using the work of Germano [3], we extend this field to general helical geometries in Section 2.3.

#### **2.1 A general pipe coordinate system**

We introduce a cross-sectionally defined coordinate system  $(x, y, s)$  as shown in Figure (2.1). Let  $\vec{q}$  be a path parameterizing the center-line of the pipe, and let  $s$  represent the arc-length along the path. We define the  $x$  coordinate to point in the opposite direction of the inward-pointing normal of  $\vec{s}$ , and the  $y$  coordinate to point in the direction of the binormal. This system is equivalent to labeling each cross section with a value of  $s$  and mapping the particles old  $x$  and  $y$  positions into the new cross-section. For some equations of fluid motion, it may be convenient to replace  $t$  derivatives with  $s$  derivatives in the equations of motion, as particles travel in only one direction for increasing time.

As an example, consider the straight pipe with (non-dimensional) cross-sectional radius one. We can parameterize the center-line by a straight line

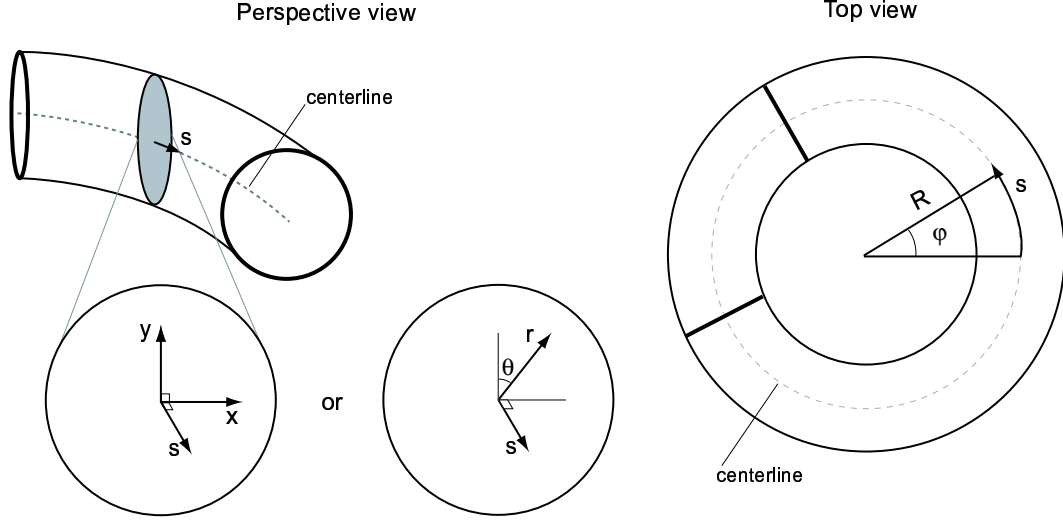


Figure 2.1: The coordinates are defined in relation to the Frenet frame of path  $\vec{s}$  parameterizing the center-line of the pipe, with  $x$  oriented opposite of the inward-pointing normal and  $y$  oriented along the binormal. Note that the distance traveled along  $\vec{s} = s = R\varphi$ , where  $R$  is the radius of curvature.

path, meaning that the  $s$ -coordinate is now just another spatial dimension globally orthogonal to  $x$  and  $y$ . In fact, since the normal and binormal do not change orientation, the cross-sectional definition is just a standard euclidian system. Note that for other paths, the coordinates are only *locally* orthogonal. The orientation of  $x$  and  $y$  in a given cross-section is not necessarily the same as the orientation of  $x$  and  $y$  any other cross-section.

The fluid motion in the straight pipe obeys

$$H_t + u_0(1 - r^2)H_s = D\nabla^2 H, \quad (2.1)$$

where  $u_0$  is the velocity of the pipe at the center-line and  $r$  is the radial distance from the center-line to a point in the cross-section. This is the same as equation (1.4) for Poiseuille flow. Normally, the centerline velocity  $u_0$  is much larger than  $D$ , as the advective forces due are much more important than the diffusive forces. This situation and its anomalous mixing regimes are

investigated in depth in Latini & Bernoff [7].

## 2.2 Torodial pipe flow equations

We ignore the effects of diffusion and concentrate on describing the velocity field  $\vec{u}$  inside the pipe. In the torodial pipe, the pipe center-line  $\vec{q}$  has constant curvature  $\kappa$  and no torsion. For this derivation it is convenient to introduce radial coordinates  $(r, \theta)$  into the cross-section. Let  $\vec{u} = (u, v, w) = (\dot{s}, \dot{r}, \dot{\theta})$ . Following Ward-Smith [11], we write the first fundamental form for this coordinate system:

$$(dq)^2 = \left(1 + \frac{r}{R} \sin \theta\right)^2 (ds)^2 + (dr)^2 + (r)^2 (d\theta)^2. \quad (2.2)$$

Notice that this is nearly a cylindrical system. The different scale factor on  $ds$  arises from the curvature of the pipe causing a point following a line in  $s$  to also change position in the cross-section. We now assume the flow to be steady and viscous. The problem is governed by the steady, incompressible Navier-Stokes continuity and momentum equations

$$\nabla \cdot \vec{u} = 0 \quad (2.3)$$

and

$$\vec{u} \cdot \nabla \vec{u} = \frac{1}{\rho} \nabla P + \nu \nabla^2 \vec{u}, \quad (2.4)$$

where  $P$  is the pressure gradient driving the flow in the pipe,  $\rho$  is the density of the fluid, and  $\nu = \mu/\rho$  is the kinematic viscosity of the fluid. Assuming that the flow is laminar, we omit the partial derivatives of  $\vec{u}$  with respect to  $s$ . For (2.3), we have

$$\frac{\partial v}{\partial r} + \frac{1}{r} \frac{\partial w}{\partial \theta} + \frac{v}{r} + \frac{v \sin \theta + w \cos \theta}{R + r \sin \theta} = 0, \quad (2.5)$$

and for (2.4), we have the three equations

$$\begin{aligned}
v \frac{\partial u}{\partial r} + \frac{w}{r} \frac{\partial u}{\partial \theta} + \frac{u(v \sin \theta + w \cos \theta)}{R + r \sin \theta} \\
= -\frac{1}{\rho} \left( \frac{R}{R + r \sin \theta} \right) \frac{\partial P}{\partial s} + \nu \left[ + \frac{\partial^2 u}{\partial r^2} + \frac{1}{r^2} \frac{\partial^2 u}{\partial \theta^2} - \frac{u}{R + r \sin \theta} + \frac{1}{r} \frac{\partial u}{\partial r} \right. \\
\left. + \frac{1}{r} \frac{\partial u}{\partial r} + \frac{1}{R + r \sin \theta} \left( \sin \theta \frac{\partial u}{\partial r} + \frac{\cos \theta}{r} \frac{\partial u}{\partial \theta} \right) \right],
\end{aligned} \tag{2.6}$$

$$\begin{aligned}
v \frac{\partial v}{\partial r} + \frac{w}{r} \frac{\partial v}{\partial \theta} - \frac{w^2}{r} - \frac{u^2 \sin \theta}{R + r \sin \theta} \\
= -\frac{1}{\rho} \frac{\partial P}{\partial r} + \nu \left[ \frac{\partial^2 v}{\partial r^2} + \frac{1}{r} \frac{\partial v}{\partial r} + \frac{v}{r^2} + \frac{1}{r^2} \frac{\partial^2 v}{\partial \theta^2} - \frac{2}{r^2} \frac{\partial w}{\partial \theta} \right. \\
\left. + \frac{1}{R + r \sin \theta} \left( \sin \theta \frac{\partial v}{\partial r} + \frac{\cos \theta}{r} \frac{\partial v}{\partial \theta} - \frac{w \cos \theta}{r} \right) \right. \\
\left. - \frac{\sin \theta}{(R + r \sin \theta)^2} (v \sin \theta + w \cos \theta) \right],
\end{aligned} \tag{2.7}$$

and

$$\begin{aligned}
v \frac{\partial w}{\partial r} + \frac{w}{r} \frac{\partial w}{\partial \theta} - \frac{vw}{r} - \frac{u^2 \cos \theta}{R + r \sin \theta} \\
= -\frac{1}{r\rho} \frac{\partial P}{\partial \theta} + \nu \left[ \frac{\partial^2 w}{\partial r^2} + \frac{1}{r} \frac{\partial w}{\partial r} + \frac{w}{r^2} + \frac{1}{r^2} \frac{\partial^2 w}{\partial \theta^2} \right. \\
\left. - \frac{2}{r^2} \frac{\partial v}{\partial \theta} + \frac{\sin \theta}{R + r \sin \theta} \frac{\partial w}{\partial r} + \frac{\cos \theta}{R + r \sin \theta} \left( \frac{1}{r} \frac{\partial w}{\partial \theta} + \frac{v}{r} \right) \right. \\
\left. - \frac{\cos \theta}{R + r \sin \theta} (v \sin \theta + w \cos \theta) \right].
\end{aligned} \tag{2.8}$$

Let  $\epsilon = a/R$ . Assuming that the radius of curvature is much larger than the radius of the pipe, i.e.  $R \gg a$  or  $\epsilon \ll 1$ , the behavior of this system is a perturbation of Poiseuille flow:

$$u = A(a^2 - r^2) + \tilde{u}; \quad v = 0 + \tilde{v}; \quad w = 0 + \tilde{w}; \quad \frac{P}{\rho} = Cs + \frac{\tilde{p}}{\rho}, \tag{2.9}$$

where A and C are constants and the tilde-marked terms are small perturbations. If the tilde terms are small, then the product of tilde terms can be safely

neglected. Rewriting equations (2.5)–(2.8) using the perturbation in (2.9), we have

$$\frac{\partial \tilde{v}}{\partial r} + \frac{\tilde{v}}{r} + \frac{1}{r} \frac{\partial \tilde{w}}{\partial \theta} = 0, \quad (2.10)$$

$$\begin{aligned} -2Ar\tilde{v} = & (1 - r\epsilon \sin \theta) \left( C + \frac{1}{\rho} \frac{\partial \tilde{p}}{\partial s} \right) \\ & + \nu \left( \frac{\partial^2}{\partial r^2} + \frac{1}{r} \frac{\partial}{\partial r} \frac{1}{r^2} \frac{\partial^2}{\partial \theta^2} \right) (A(a^2 - r^2) + \tilde{u}) \end{aligned} \quad (2.11)$$

$$\begin{aligned} & + \nu \epsilon \left[ \left( \frac{\partial}{\partial r} + \frac{1}{r} \right) (A(a^2 - r^2) \sin \theta) + \frac{1}{r} \frac{\partial}{\partial \theta} (A(a^2 - r^2) \cos \theta) \right], \\ -\epsilon A^2 (a^2 - r^2)^2 \sin \theta = & \frac{1}{\rho} \frac{\partial \tilde{p}}{\partial r} - \frac{\nu}{r} \frac{\partial}{\partial \theta} \left( \frac{\partial \tilde{w}}{\partial r} + \frac{\tilde{w}}{r} - \frac{1}{r} \frac{\partial \tilde{v}}{\partial \theta} \right), \end{aligned} \quad (2.12)$$

and

$$-\epsilon A^2 (a^2 - r^2)^2 \cos \theta = -\frac{1}{r} \frac{1}{\rho} \frac{\partial \tilde{p}}{\partial \theta} + \nu \frac{\partial}{\partial r} \left( \frac{\partial \tilde{w}}{\partial r} + \frac{\tilde{w}}{r} - \frac{1}{r} \frac{\partial \tilde{v}}{\partial \theta} \right). \quad (2.13)$$

where all higher-order tilde terms and terms second order or higher in  $\epsilon$  have been dropped. In equation (2.11), we have both “large” and “small” terms.

We can solve for  $C$  by balancing the large terms:

$$0 = C - 2A\nu - 2A\nu, \quad (2.14)$$

and so,

$$C = -4A\nu. \quad (2.15)$$

Equation (2.11) becomes

$$-2Ar\tilde{v} = \frac{1}{\rho} \frac{\partial \tilde{p}}{\partial s} - \epsilon(6\nu Ar \sin \theta) + \nu \left( \frac{\partial^2 \tilde{u}}{\partial r^2} + \frac{1}{r} \frac{\partial \tilde{u}}{\partial r} + \frac{1}{r^2} \frac{\partial^2 \tilde{u}}{\partial \theta^2} \right). \quad (2.16)$$

Now we separate variables. Let a circumflex represent a quantity which is a function of  $r$  alone. We make the substitutions

$$\tilde{u} = \hat{u} \sin \theta, \quad (2.17)$$

$$\tilde{v} = \hat{v} \sin \theta, \quad (2.18)$$

$$\tilde{w} = \hat{w} \cos \theta, \quad (2.19)$$

$$\frac{\tilde{p}}{\rho} = \hat{p} \sin \theta, \quad (2.20)$$

into equations (2.10), (2.12), (2.13), and (2.16). Using a no slip boundary condition ( $\vec{u} = 0$  at  $r = a$ ), we can solve these equations for the fluid velocity. For convenience, we rescale velocity by  $C/(4\nu)$  and distance by  $a$ . This gives

$$u = 2(1 - r^2) \left( 1 - \epsilon \frac{3}{4} r \sin \theta + \epsilon \frac{(Re)}{11520} r \sin \theta [19 - 21r^2 + 9r^4 - r^6] \right), \quad (2.21)$$

$$v = \epsilon \frac{(Re)}{144} \sin \theta (4 - r^2)(1 - r^2)^2, \quad (2.22)$$

$$w = \epsilon \frac{(Re)}{144} \cos \theta (1 - r^2)(4 - 23r^2 + 7r^4), \quad (2.23)$$

where  $(Re) = 2U/\nu$  is the Reynolds number. These equations have only two parameters,  $\epsilon$  and  $(Re)$ . Following our perturbation assumption,  $\epsilon$  is small compared to  $2(1 - r^2)$ , leading us to discard the  $\epsilon$  terms in the equation for  $u$ . Note that we keep terms that are first order in  $\epsilon$  for  $v$  and  $w$ , as these terms qualitatively change the flow from Poiseuille flow. We will want to find a stream function for the velocity field in the next chapter. For this, it is easier to use Cartesian coordinates in the cross-section. We make the change of variables  $x = r \sin \theta$  and  $y = r \cos \theta$ . The above equations can be written in the following form due to Aref et.al. [5]:

$$\begin{aligned} \dot{x} &= \frac{(Re)\epsilon}{144} \left[ h(r) + \frac{y^2}{r} h'(r) \right], \\ \dot{y} &= -\frac{(Re)\epsilon}{144} \frac{xy}{r} h'(r), \\ \dot{s} &= 2(1 - r^2). \end{aligned} \quad (2.24)$$

The function  $h(r)$  is common to both  $\dot{x}$  and  $\dot{y}$  and is given by

$$h(r) = \frac{1}{4}(4 - r^2)(1 - r^2)^2. \quad (2.25)$$

If we rescale time by  $(Re)\epsilon/144$  and rescale  $s$  by  $(Re)\epsilon/288$  we arrive finally at

$$\dot{x} = h(r) + \frac{y^2}{r} h'(r),$$

$$\begin{aligned}\dot{y} &= -\frac{xy}{r}h'(r), \\ \dot{s} &= 1 - r^2.\end{aligned}\tag{2.26}$$

Examining these equations, we see that the centripetal force on the fluid induces rotating velocity fields in  $x$  and  $y$ , but that the behavior in the  $s$  direction is just Poiseuille flow. Figure (3.2) in the next chapter shows the streamlines of this flow field.

### 2.3 Helical pipe flow equations

Now we will extend the previous equations to situations with both constant curvature  $\kappa$  and constant torsion  $\tau$ . Examining the geometry reveals that re-using our previous toroidal coordinate system results in a first fundamental form of

$$(dq)^2 = [(1 - \kappa r \sin \theta)^2 + \tau^2 r^2](ds)^2 + (dr)^2 + r^2(d\theta)^2 + 2\tau^2 ds d\theta,\tag{2.27}$$

which is not orthogonal due to the  $ds d\theta$  term. However, if we include a  $\tau s$  rotation, we can create terms to cancel the non-orthogonal piece and create an orthogonal system:

$$(dq)^2 = [1 - \kappa r \sin(\theta + \tau s)](ds)^2 + (dr)^2 + r^2(d\theta)^2.\tag{2.28}$$

Germano [3] showed that the flow in this coordinate system has only a second order dependence on  $\tau$ . Thus, we can use our formula for flow in the toroidal pipe, (2.26), by changing basis to the new helical coordinate system, (2.28), to describe the flow at leading order. That is, the toroidal flow field is present in each cross-section of the helical pipe, but the  $x$ - $y$  coordinates it is defined with

respect to are rotating as the binormal rotates along path  $\vec{q}$ :

$$\dot{x} = h \cos(\lambda s) + \frac{h'}{r} y x \sin(\lambda s) + \frac{h'}{r} y^2 \cos(\lambda s) \quad (2.29)$$

$$\dot{y} = - \left( h \sin(\lambda s) + \frac{h'}{r} y x \cos(\lambda s) + \frac{h'}{r} x^2 \sin(\lambda s) \right) \quad (2.30)$$

$$\dot{s} = 1 - r^2. \quad (2.31)$$

where the geometry parameters have been combined into  $\lambda = q_0 \tau / \kappa$  and  $h = h(r)$  as defined in (2.25). The scale-factor  $q_0 = 144\nu/U$  balances the rescaling of  $s$ . Like the torus, there is a rotating velocity field in the cross-section, but there is also a rotation of the toroidal velocity field. Plots of the streamlines of this flow field are shown in Figure (3.2), and Figure (4.3) shows the effect of the flow on a simple initial condition.

## Chapter 3

### Stream functions for toroidal and helical pipe flow fields

In this section, we transform the flow field for the helical pipe into a Poincaré map between cross-sections. This map provides insight into the nature of the DEs and helps to clarify the nature of the flow when  $\lambda$  is large. Rather than construct the map directly, we will develop it by constructing a stream function for the flow. Section 3.1 details a method for the general construction of a stream function, and Section 3.2 uses this method to find the toroidal and helical stream functions. Finally in Section 3.3 we discuss the information provided by the helical stream function.

#### **3.1 A method for creating stream functions**

Suppose the motion of some particle was prescribed by  $\dot{x} = f(x, y)$  and  $\dot{y} = g(x, y)$ . We want to construct a stream function  $\psi$  such that

$$\psi_x = -g(x, y) \tag{3.1}$$

and

$$\psi_y = f(x, y), \tag{3.2}$$

where the subscript represents a partial derivative. Working directly, we can integrate (3.1) to get

$$\psi = \int f(x, y)dy + w(x),$$

where  $w(x)$  is an unknown function of  $x$  from the integration. To find  $w(x)$ , we will make use of property (3.2) by differentiating with respect to  $x$ :

$$\psi_x = \int f_x \, dy + w_x = -g(x, y).$$

Now we can see that

$$w_x = -g - \int f_x \, dy,$$

and so

$$w = - \int g \, dx - \iint f_x \, dy \, dx.$$

Thus, our stream function is

$$\psi = \int f(x, y) \, dy - \int g \, dx - \iint f_x \, dy \, dx. \quad (3.3)$$

From the derivation, it is clear that (3.3) obeys Properties (3.1) and (3.2). Note that if  $f_x = g_y$ , then  $\psi$  collapses to only the first term in Equation (3.3).

### 3.2 Deriving the stream functions

Both the toroidal and the helical flow fields are simple enough to permit the use of the above technique for constructing stream functions.

For the torus, the stream function for the Poincaré map and the stream function for the flow field are identical, as the Dean Equations describe all of the effects of the flow. We apply the formula (3.3) to equation (2.26). This yields

$$\psi_{torus} = \int h + \frac{h'}{r} y^2 \, dx + \int \frac{h'}{r} xy \, dy - \iint \frac{\partial}{\partial x} \left( h + \frac{h'}{r} y^2 \right) \, dy \, dx.$$

Notice that  $f_x = g_y$  in this problem. Thus, the solution reduces to

$$\psi_{torus} = \frac{y}{4} (4 - r^2) (1 - r^2)^2 = yh, \quad (3.4)$$

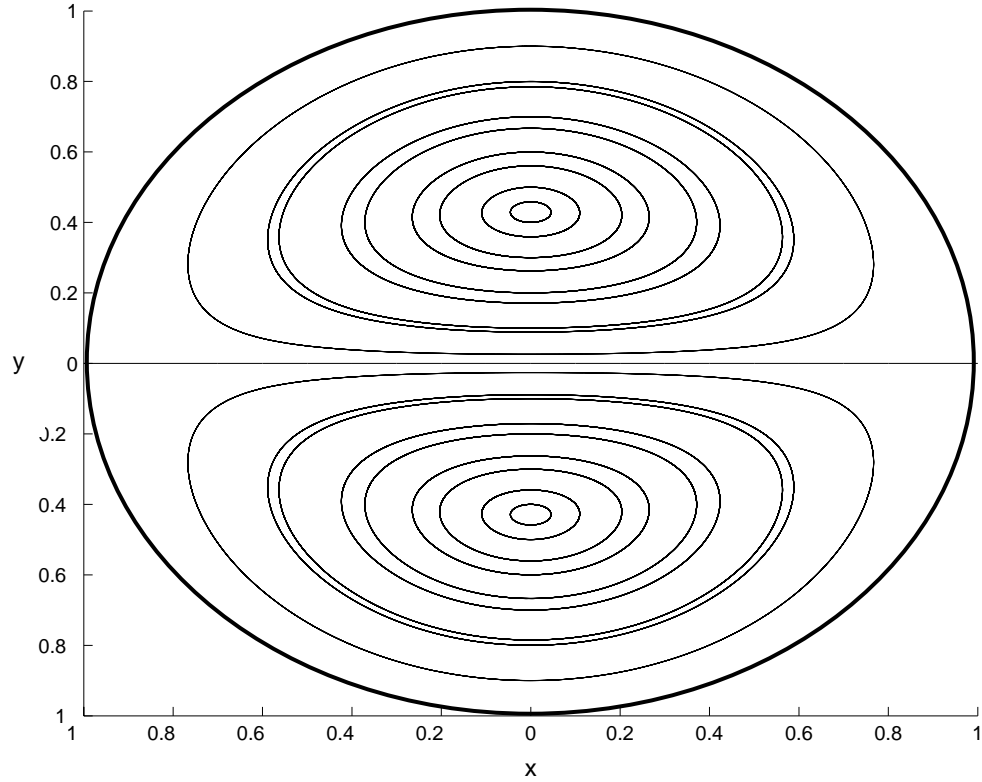


Figure 3.1: The streamlines for the toroidal velocity field are symmetric about the  $x$ -axis.

where  $h = h(r)$  defined in equation (2.25). The toroidal stream function depends on  $y$  and  $r$ , but not  $x$ . It is symmetric about the  $x$ -axis and varies at different values of  $y$ . A plot of the level sets of  $\psi_{torus}$  is shown in Figure 3.2.

In the case of the helix, torsion has no leading-order effect on the flow. However, the orientation of the flow changes in each cross-section due to the twist in the helix. A Poincaré map for this problem is the composition of the  $\tau s$  rotation of the coordinates described in equation (2.28) with the Dean Equation stream function.

To find this stream function, we will first rewrite the helix DEs to remove time dependence, then we will construct the stream function.

In the Dean Equations,

$$\begin{aligned}\dot{x} &= h + y^2 \frac{h'}{r} \\ \dot{y} &= -xy \frac{h'}{r} \\ \dot{s} &= 1 - r^2,\end{aligned}$$

we note that  $\dot{s}$  only depends on  $r$  and will not be effected by any rotation in the cross-section. Also, since neither  $t$  nor  $s$  appear in the equations for  $\dot{x}$  and  $\dot{y}$ , we can rewrite the equations by substituting an  $s$  derivative for the time derivatives by dividing by  $\dot{s}$ . This gives us

$$\frac{\partial x}{\partial s} = (h + y^2 \frac{h'}{r}) / (1 - r^2) \quad (3.5)$$

$$\frac{\partial y}{\partial s} = xy \frac{h'}{r} / (1 - r^2). \quad (3.6)$$

Next, we will adopt a vector notation for conciseness. Let  $\vec{x} = (x \ y)^T$  be the unrotated coordinates in the current cross-section (ie, the coordinates of the Dean Equations), and let  $\vec{f} = (\frac{\partial x}{\partial s} \ \frac{\partial y}{\partial s})^T$ . Define

$$R = \begin{pmatrix} \cos(\lambda s) & \sin(\lambda s) \\ -\sin(\lambda s) & \cos(\lambda s) \end{pmatrix},$$

where the angle  $\lambda s$  is the angle between the binormal in the cross-section  $s$  as measured against the binormal in the initial cross-section. Let  $\vec{X} = (X \ Y)^T$  be the rotated coordinates defined by  $\vec{X} = R\vec{x}$ . Now we change (3.5) to the rotated coordinates by differentiating the coordinate relationship with respect to  $s$ , arriving at

$$\frac{\partial \vec{X}}{\partial s} = \frac{\partial R}{\partial s} \vec{x} + R \frac{\partial \vec{x}}{\partial s}. \quad (3.7)$$

To find  $\frac{\partial \vec{x}}{\partial s}$ , we conjugate  $\vec{f}$  by  $R^{-1}$  and repeatedly use our coordinate relation-

ship to see that

$$\begin{aligned}
\frac{\partial \vec{X}}{\partial s} &= \frac{\partial R}{\partial s} \vec{x} + RR^{-1} \vec{f}(R\vec{x}). \\
&= \frac{\partial R}{\partial s} R^{-1} \vec{X} + \vec{f}(\vec{X}) \\
&= \lambda \begin{pmatrix} 0 & -1 \\ 1 & 0 \end{pmatrix} \vec{X} + \vec{f}(\vec{X}).
\end{aligned} \tag{3.8}$$

Translating (3.8) out of vector notation, we have

$$\frac{\partial X}{\partial s} = -\lambda Y + (h + Y^2 \frac{h'}{r}) / (1 - r^2) \tag{3.9}$$

$$\frac{\partial Y}{\partial s} = \lambda X + XY \frac{h'}{r} / (1 - r^2) \tag{3.10}$$

Now we can find a stream function using formula (3.3):

$$\psi_{helix} = \int \frac{\partial X}{\partial s} dY - \int \frac{\partial Y}{\partial s} dX - \iint \frac{\partial}{\partial X} \left( \frac{\partial X}{\partial s} \right) dY dX.$$

Which reduces to

$$\begin{aligned}
\psi_{helix} &= \frac{\lambda r^2}{2} \left( \frac{r^2}{2} - 1 \right) + \frac{y}{4} (4 - r^2) (1 - r^2)^2 \\
&= \frac{\lambda r^2}{2} \left( \frac{r^2}{2} - 1 \right) + \psi_{torus}.
\end{aligned} \tag{3.11}$$

Plots of the streamlines for various values of  $\lambda$  appear in Figure 3.2.

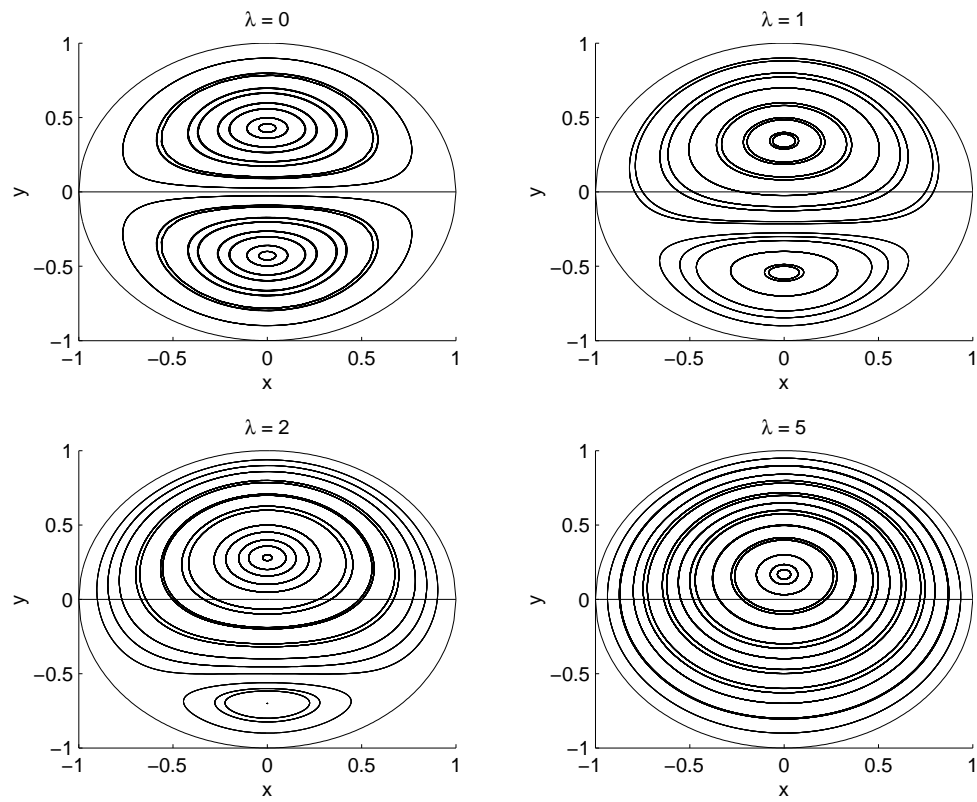


Figure 3.2: Show here are streamlines for various values of  $\lambda$ . Clockwise from the upper left:  $\lambda = 0$ ,  $\lambda = 1$ ,  $\lambda = 2$ ,  $\lambda = 5$ .

### **3.3 Consequences of the helical stream function**

In equation (3.11),  $\psi_{helix}$  is just a perturbation of  $\psi_{torus}$ . For  $\lambda = 0$ , we recover  $\psi_{torus}$ . For,  $\lambda \gg 1$ , the  $\lambda$  dependent piece is radially symmetric, implying that the streamlines become circles centered about the origin. We can understand this limit to be flow in a straight pipe measured in a (now nonsensical) helical coordinate system. The rotation of each particle on a circular streamline exactly counteracts the rotation of the helical coordinate system, implying that particles actually do not actually move in  $x$  or  $y$  when changing cross-section, as is the case in the straight pipe.

## Chapter 4

### Numerical methods

Recall from equation (1.4), in the Eulerian (lab) frame, the advection-diffusion problem can be written

$$H_t + \vec{u} \cdot \nabla H = D \nabla^2 H, \quad (4.1)$$

where  $H$  is the scalar distribution, and  $\vec{u}$  is the velocity of the fluid at any point. This equation consists of two pieces: advection and diffusion. They can be written separately as

$$H_t + \vec{u} \cdot \nabla H = 0 \quad (4.2)$$

and

$$H_t = D \nabla^2 H. \quad (4.3)$$

In our simulation, we want to take advantage of this splitting by simulating the effects of advection and diffusion separately. The general framework is as follows: we inject a large number of particles into the flow at time  $t = 0$  in some initial configuration (all at a single point, spread evenly around a cross-section, etc). Then we simulate the effects of (4.2), followed by a simulation of (4.3) to compute new particle positions. This Monte Carlo approach can be used to generate statistics about the discrete distribution of the particles at each time-step that approximate the continuous valued  $H$  with arbitrary accuracy. These data report on the degree of mixing of the released particles. Note that since our particles simulate passive scalars (such as dye molecules, or even heat if the pipe is perfectly insulated), they *do not interact*. Particles

may lie atop one another in our simulation. This can be physically justified by noting that our spacial scale is very large compared to the size of a dye molecule, so multiple particles in the same space could represent a particularly high concentration of dye. In the case of particles representing quantities of heat, this super-position of particles simply represents a “hot spot”. This chapter will develop methods for solving the advection problem in Section 4.1, methods for solving the diffusion problem in Section 4.2, and the combination of these methods will be discussed in Section 4.3, along with an analysis of the error committed. Finally, Section 4.4 will present pictures of the simulation in action.

#### **4.1 *Simulating advection***

To simulate advection, the movement of suspended particles in a fluid flow, we must know the velocity at each point where there is a particle. To advect scalars in a flow would require solving the Navier-Stokes Equations on a grid in the pipe to determine the velocity of the flow at each point where there is a particle, or knowing  $\vec{u}$  and solving (4.2). The Navier-Stokes Equations are PDEs and are slow to solve numerically, while solving (4.2) involves a straightforward ODE integration. The boundary conditions imposed by the pipe walls are already included in the formulation of  $\vec{u}$ , sparing routines using this method the time required to calculate their effects. The catch is that we must be able to compute  $\vec{u}$  analytically before the simulation. Fortunately, we have already found  $\vec{u}$  in (2.29) for our problem. We can then advect particles by splitting (4.2) into a set of ODEs. If  $\vec{u} = u\hat{x} + v\hat{y} + w\hat{s}$ , then let

$$\dot{x} = u, \quad \dot{y} = v, \quad \dot{s} = w. \tag{4.4}$$

Using a fourth order Runge-Kutta method, we can solve (4.4) for each particle individually. This simulation method represents a good balance between

accuracy and speed. In practice, we advect all of the particles each time-step, rather than advecting one particle through all of the required time-steps before starting to move the next particle. This algorithm allows us to calculate statistics based on the distribution at each time-step.

## 4.2 *Simulating diffusion*

Rather than solve the diffusion equation (4.3), we will simulate diffusion stochastically through a random particle walk. The random walk formulation of diffusion is a very physical one: particles diffuse because of random collisions imparting random velocities. The net effect of this is to force particles apart. At each time-step, a particle randomly moves some distance from its old position according to

$$\vec{x}_{n+1} = (x_t + \Delta x)\hat{i} + (y_t + \Delta y)\hat{j} + (s_t + \Delta s)\hat{k}, \quad (4.5)$$

where the subscript represents the time-step. Determining  $\Delta\vec{x} = \Delta x\hat{i} + \Delta y\hat{j} + \Delta s\hat{k}$  determines the nature of the random walk. To simulate diffusion properly, we want  $\Delta\vec{x}$  to be a normal random variable with mean 0 and standard deviation  $\sigma_\Delta$  the same as the width of our gaussian solution to (4.3):

$$\sigma_\Delta = \sqrt{2Dh}, \quad (4.6)$$

where  $h$  is the size of a time-step. This is equivalent to taking three independent random walks in the  $x$ ,  $y$  and  $s$  directions, all with the same  $\sigma_\Delta$ . With enough particles and many timesteps, the distribution will spread diffusively. Notice that if particle  $p$  has diffused a small distance away from particle  $q$ , then the chance that  $\Delta\vec{x}$  points back toward  $q$  in the next random walk is exceedingly small.

In this particular application, there are two difficulties in applying the random walk approach:

- (1) the coordinates are not globally orthogonal, and
- (2) there are walls stopping particles from leaving the pipe.

First, we examine problem (1). Since the  $s$  coordinate is only locally orthogonal, diffusion in the  $s$  direction must be handled in a special way. Our coordinates  $x$  and  $y$  are defined in relation to the cross-section. Changing  $s$  changes this cross-section, so the location of the particle in  $x$  and  $y$  must be corrected to account for this (in addition to the independent random walks in these directions). For the torus ( $\lambda = 0$ ), the corrections can be computed easily. For  $\lambda > 0$ , these corrections become more involved. To simplify and speed our algorithm, we will choose to ignore diffusion in the  $s$  direction. Since the fluid velocity in the  $s$  direction is order 1, and  $D \ll 1$ , this assumption does not introduce much error. A more precise answer involves analyzing the advection diffusion equation (4.1). Working in the toroidal coordinate system from Chapter 2, we can split the vector operators into  $s$  and cross-sectional pieces  $(r, \theta)$ . This gives

$$\begin{aligned}
H_t + \frac{R}{R + r \sin \theta} u H_s + v H_r + \frac{w}{r} H_\theta = \\
D \left( \frac{R}{R + r \sin \theta} \right)^2 H_{ss} + D \left[ \frac{1}{r} H_r + \frac{\sin \theta}{R + r \sin \theta} H_r + H_{rr} \right] \\
+ D \left[ \frac{\cos \theta}{r(R + r \sin \theta)} H_\theta + \frac{1}{r^2} H_{\theta\theta} \right].
\end{aligned} \tag{4.7}$$

As before, we let  $\epsilon = a/R$ . Since in our final model, we rescale  $t$  and  $s$ , we insert that rescaling into this analysis and collect the  $\epsilon$  terms

$$\begin{aligned}
H_t + \frac{2}{1 + r\epsilon \sin \theta} u H_s + \frac{1}{\epsilon} v H_r + \frac{w}{r\epsilon} H_\theta = \\
4\epsilon D \left( \frac{1}{1 + r\epsilon \sin \theta} \right)^2 H_{ss} + \frac{D}{\epsilon} \left[ \frac{1}{r} H_r + \epsilon H_r + H_{rr} \right] \\
+ \frac{D}{\epsilon} \left[ \frac{\cos \theta}{rR} H_\theta + \frac{1}{r^2} H_{\theta\theta} \right].
\end{aligned} \tag{4.8}$$

Let  $v' = \epsilon v$ ,  $w' = \epsilon w$ , and  $D' = D/\epsilon$ . Then the above becomes

$$H_t + \frac{2}{1 + r\epsilon \sin \theta} u H_s + v' H_r + \frac{w'}{r} H_\theta = 4\epsilon D \left( \frac{1}{1 + r\epsilon \sin \theta} \right)^2 H_{ss} + D' \left[ \frac{1}{r} H_r + \epsilon H_r + H_{rr} \right] + D' \left[ \frac{\cos \theta}{rR} H_\theta + \frac{1}{r^2} H_{\theta\theta} \right]. \quad (4.9)$$

Note that since  $R \gg a$ ,  $\epsilon = a/R$  is small. Only the  $s$  diffusion term is first-order in  $\epsilon$ . All other terms are lower order. Dropping the lower-order terms results in

$$H_t + 2uH_s + \vec{u}_\perp \cdot \nabla H = D' \nabla_\perp^2 H, \quad (4.10)$$

where the perpendicular symbol denotes vector operators operating in the cross-section only. This equation is a simplified form of the advection-diffusion equation from before, but it is missing longitudinal diffusion. It is clear from our scaling analysis that we can safely ignore diffusion in the  $s$  direction.

But why not ignore diffusion in the other two directions? From (4.8) we see that the  $r$  and  $\theta$  terms are both  $O(1)$ , so quantitative they are important. The qualitative answer is that cross-sectional diffusion gives particles a mechanism by which they can change streamlines (see Section 3.2). Since each streamline samples different positions in the pipe's cross-section, changing streamlines changes a particle's velocity down the pipe. This results in a qualitatively different behavior. Section 5.4 has a more developed explanation of this phenomena.

Now we will solve problem (2). To prevent particles from diffusing outside of the pipe, we must simulate some sort of boundary interaction. Since the random walk diffusion is already simulating the effects of particle-on-particle collisions, the sensible approach is to have particles which try to diffuse outside of the pipe boundary instead reflect off the pipe wall like a billiards ball off a table edge (see Figure 4.2). Since in (1) we decided to ignore transverse

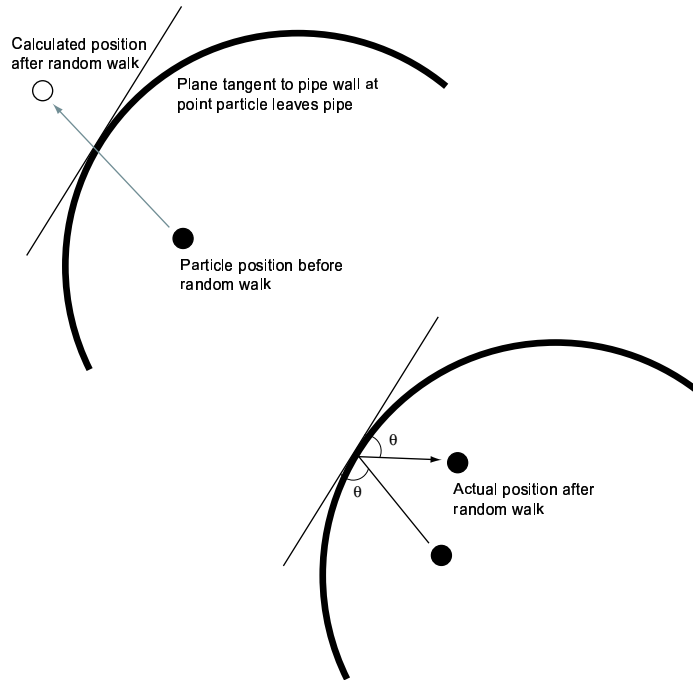


Figure 4.1: The pipe walls reflect particles that attempt to move beyond them during the random walk.

diffusion, all reflections happen on the unit circle in the cross-section. This collision should preserve the total distance the particle travels. If the  $|\Delta\vec{x}| = d$ , but the distance in the  $\Delta\vec{x}$ -direction to the wall is  $d_1 < d$ , then the particle will reflect and move a distance  $d_2 = d - d_1$ . Should moving a distance  $d_2$  take the particle outside of the pipe again, another reflection is performed, and so on.

### 4.3 Composing advection and diffusion: error analysis

Now that we have adapted random-walk diffusion to suit our problem, we must concern ourselves with combining advection and diffusion. Since diffusion can change the streamline that a particle inhabits, the order of these operations has an impact on the outcome of the problem. In general, for each time-step

$h$ , we need to diffuse the particle for a total time  $h$  and advect it for a total time  $h$ . However, these processes occur simultaneously in equation (4.1), so in running them independently, we incur some error. Following the result of Bernoff & Lingeitch [9], we use a split step method to reduce this error. The advection step is divided into two sub-steps of length  $h/2$  and the diffusion step is inserted between them. The overall process is advection for a time  $h/2$ , followed by diffusion for a time  $h$ , followed by advection for a time  $h/2$ . This method introduces  $h^2$  error. We will refer to this error as the *separation error*.

Two other sources of error are also important. First, Runge-Kutta 4 introduces  $O(h^4)$  error, which is much smaller than the error incurred by the separation of the two processes and therefore unimportant. The second source, the random-walk approximation to diffusion, requires some analysis. In general, we will not be concerned with errors in a particle's position as much as we are concerned in the error in the width of the  $s$ -distribution of particles, characterized by  $\sigma$  (we will use this measurement in Chapter 5 to characterize the degree of mixing). To analyze the error in this variable, we can approximate the true distribution width,  $\sigma$ , with the second discrete moment in  $s$  of our particle distribution:

$$\sigma^2 \approx \frac{1}{N} \sum s^2 = q^2, \quad (4.11)$$

where the sum is the sum of the squared  $s$  distance traveled by each particle and  $N$  is the total number of particles used. The average (expected) absolute error in  $\sigma^2$  is

$$e_{abs}^2 = E((q^2 - \sigma^2)^2). \quad (4.12)$$

Using the fact that the expected value of the sum is the sum of the expected values and that that expected value of the sum of  $s^2$  is  $\sigma$ , we arrive at

$$e_{abs}^2 = \frac{1}{N} [E(s^4) - \sigma^4]. \quad (4.13)$$

The expected value of the fourth moment of  $s$  is the kurtosis. From the results in Section 1.3, we have that for  $t \gg 1/D$ , the distribution has a gaussian shape. Since the kurtosis of a gaussian is  $3\sigma^4$ , the absolute error is

$$e_{abs} = \sigma^2 \sqrt{\frac{2}{N}}, \quad (4.14)$$

which implies that the relative error is

$$e_{rel} = \frac{e_{abs}}{\sigma^2} = \sqrt{\frac{2}{N}}. \quad (4.15)$$

The error from the diffusion simulation depends on the number of particles used. At least 10000 particles are needed when  $h = 0.1$  (a moderately sized timestep  $h$ ) to keep the diffusion error on the same order of magnitude as the separation error.

#### **4.4 Flow visualization**

We can plot the position of each particle in our simulation inside of the unit disk by projecting down the  $s$ -axis. To see the effects of the streamlines for various  $\lambda$ , we will release 10000 particles in a uniform strip along the  $y$ -axis and set  $D = 0$ . Figure (4.2) shows the flow for  $\lambda = 0$ .

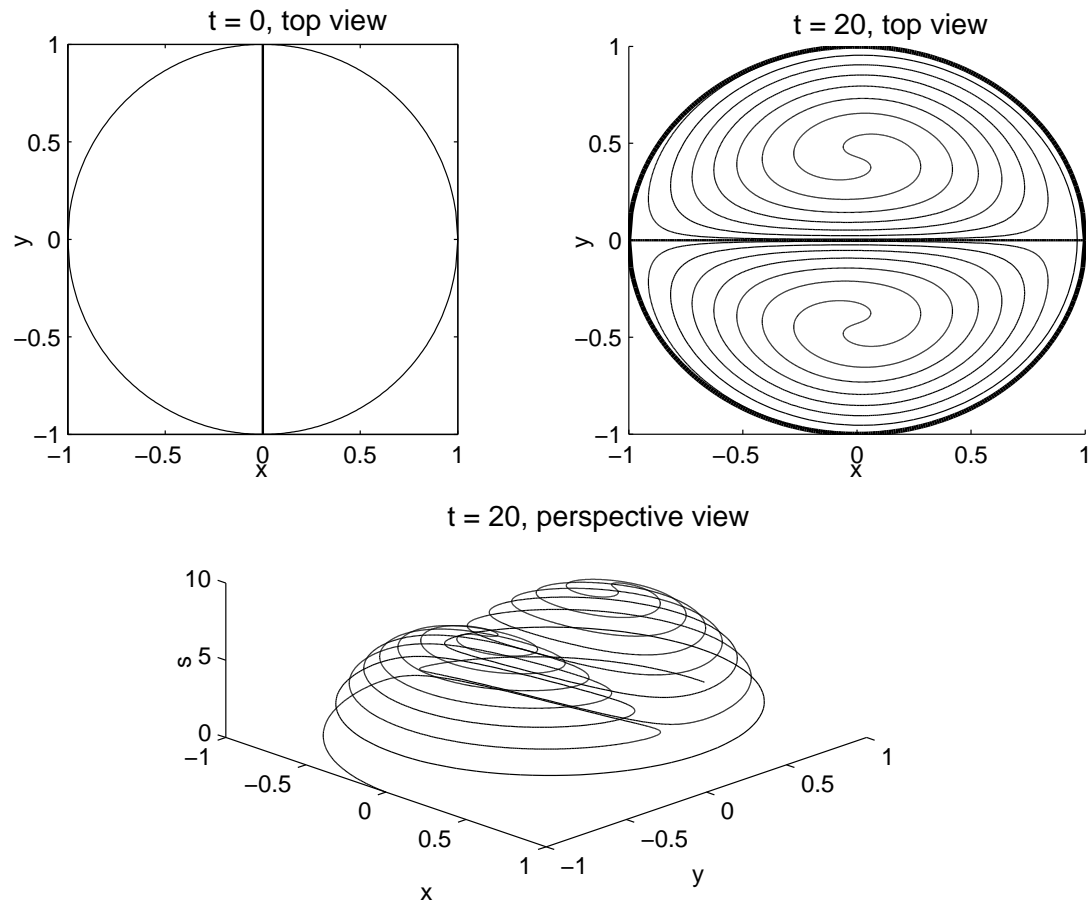


Figure 4.2: A strip of particles is released into a pipe with  $\lambda = 0$  and evolves into two counter-rotating spirals shown here projected down the  $s$ -axis. The perspective picture shows the  $1 - r^2$  profile in the  $s$  direction.

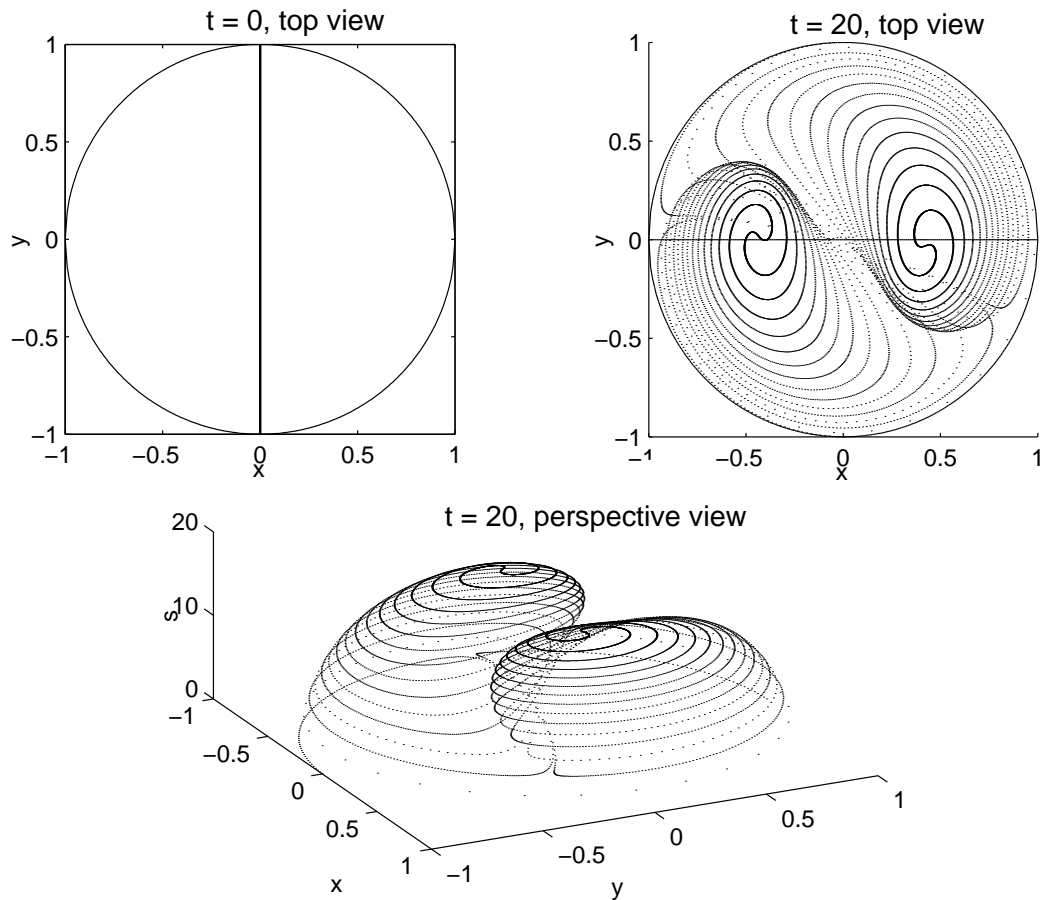


Figure 4.3: With  $\lambda = 0.1$ , the rotation of the binormal causes the centers of the two spirals shown in Figure (4.4) to orbit the cross-section.

Here the recirculation in the cross-section draws the strip into two symmetric spirals. In Figure (4.3), we repeat the experiment, but this time we add a moderate amount of torsion to the pipe ( $\lambda = 0.1$ ). Notice that in the three-dimensional projection, the two lobes of the flow field are rotating about each other.

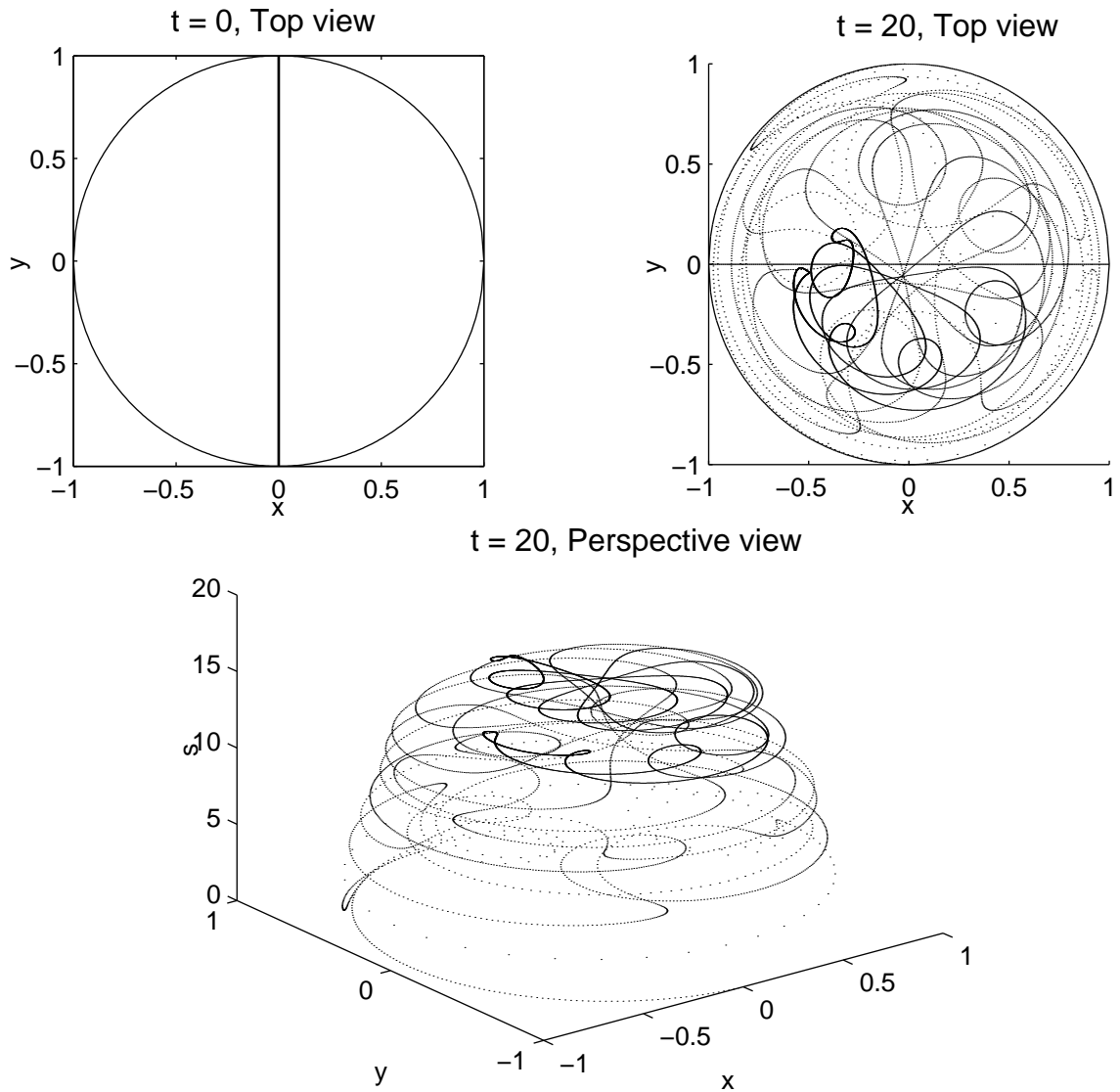


Figure 4.4: For large  $\lambda$  (here  $\lambda = 1$ ), the spiral pattern breaks down quickly.

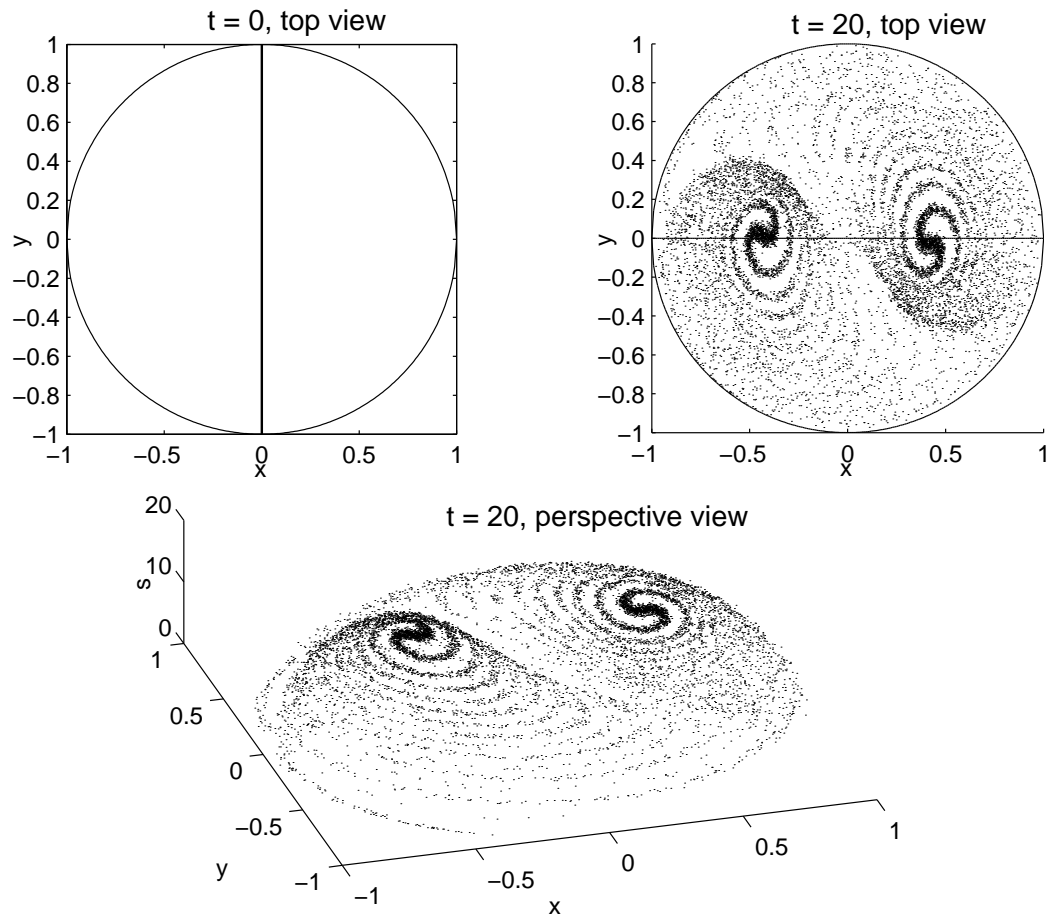


Figure 4.5: Adding a modest amount of diffusion ( $D = 10^{-5}$ ) introduces some noise into the spiral pattern, accelerating its decay.

In Figure (4.4), we have set  $\lambda = 1$ , and the dual-spiral structure is quickly destroyed by the effects of torsion. Finally, we can add diffusion back to our simulation to look at “dirty spirals”.

Figure (4.5) was run under the same system parameters as Figure (4.3), but with  $D = 10^{-5}$ . Diffusion smudges the flow pattern. The effects of this are discussed in Section 5.4.

## Chapter 5

### The effects of torsion on mixing

The helical flow system has two parameters,  $\lambda$  and  $D$ . However, we assumed that  $D$  was small through much of our work, so we can only investigate the  $\lambda$  dimension of our parameter space. Physically, this investigation shows the link between the amount of torsion in the pipe and the scaling of the various mixing regimes. A representative experiment in Section 5.1 will serve to introduce the four regimes observed in the problem. In Section 5.2, we examine the regimes with no  $\lambda$  dependence and provide explanations for their behavior. In Section 5.3, we investigate the  $\lambda$ -dependent anomalous regime and provide numerical solutions for its scaling and timescale as functions of  $\lambda$ . Finally, the  $\lambda$  dependent Taylor dispersion regime is examined and a relation between  $\lambda$  and  $D_{eff}$  is discussed.

#### 5.1 The four mixing regimes

Using the numerical method discussed in Chapter 4, we will perform an experiment on one million particles with a small dimensionless diffusivity  $D = 10^{-4}$ . To minimize initial transient behavior, the particles will be released in a uniform plane filling the pipe at  $s = 0$ . Running the simulation for  $15000 = 1.5/D$  time units, we record  $\sigma$  in the  $s$  direction for each time step. Figure (5.1) shows the results. We notice that there are found different relationships between  $\sigma$  and  $t$ . For  $D < t < t_t$ , the width  $\sigma = t/\sqrt{12}$ , where  $t_t$  is the turnover time of the cross-sectional vortices. The effects of the flow in the cross-section are not

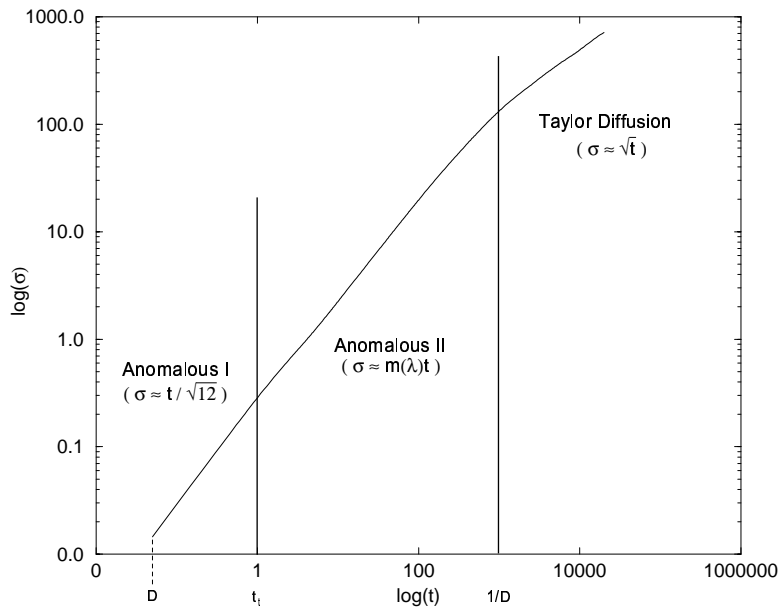


Figure 5.1: This plot of  $\sigma$  versus  $t$  reveals three mixing regimes.

yet felt and  $\sigma$  spreads like it would in a straight pipe under Poiseuille flow. We will call this mixing regime “Anomalous I”, since we observe a non-square root behavior between  $t$  and  $\sigma$ . In this regime, only the first order of the geometry of the pipe effects the flow. For  $t_t < t < 1/D$ , another linear mixing regime appears, with  $\sigma = m_\lambda t$ , where  $m_\lambda$  depends on the value of  $\lambda$ , ranging between approximately 0.2141 and 0.2887. This regime, which we will call “Anomalous II”, is influenced by the geometry of the pipe, but not the diffusivity. Next, for  $t > 1/D$ , Taylor Diffusion begins (cf. Section 1.2) and  $\sigma = \sqrt{D_{eff}t}$ , where  $D_{eff} \propto 1/D$  and depends of  $\lambda$ . In the Taylor regime, both the geometry and the diffusivity contribute to the mixing.

## 5.2 Non $\lambda$ -dependent mixing regimes

For  $t < t_t$ , we observe two regimes that do not depend on the geometry parameter  $\lambda$ . For  $t < D$ , we would expect a diffusive regime. However, the uniform cross-section release combined with the absence of diffusion in the  $s$  direction results in no noticeable change in  $\sigma$ . If  $s$ -directional diffusion were added back, we would expect to see  $\sigma = \sqrt{Dt}$ .

The behavior of the other non- $\lambda$  dependent regime can be calculated. In this case, the particles are governed by Bizet flow:

$$\dot{s} = 1 - r^2, \tag{5.1}$$

and

$$\psi = \frac{r^2}{2}. \tag{5.2}$$

In this regime, the random fluctuations of particle positions is on the order of  $D$ . Let  $\hat{x} = x + D$  represent a particle that has randomly moved a distance  $D$  from its old location. We can evaluate the error in the particle's  $s$  position arising from the assumption that we may neglect the effects of diffusion in this mixing regime. We have

$$e_D = |2xD + D^2|. \tag{5.3}$$

Thus the error is on the order of  $D$ . With the assumption that  $D$  is smaller than our simulation error, we may neglect the effects of diffusion. We can now calculate the  $s$  distribution of particles simply from (5.1) and (5.2). We want to find the slope of  $\sigma(t)$  and we proceed by averaging the concentration on the streamlines. Since we are neglecting diffusion, there is no mechanism to transport particles from their original streamline at time  $t = 0$  to any other streamline. Thus, we assume that all of the particles on a given streamline move at the average velocity of that streamline. Since all of the streamlines of  $\psi$  are circles, we have that the velocity of a streamline,  $w(r) = 1 - r^2$ . In

general, from statistics we have that

$$\sigma^2 = \langle w^2 t^2 \rangle - \langle w t \rangle^2,$$

where  $\langle \cdot \rangle$  is the expected value. Since in the Anomalous I regime,  $w$  does not truly depend on time, we have

$$\sigma^2 = m^2 t^2 = (\langle w^2 \rangle - \langle w \rangle^2) t^2. \quad (5.4)$$

We can adapt this to our problem by writing

$$m^2 = \frac{1}{\pi} \int_{\psi_-}^{\psi_+} w^2 d\psi - \frac{1}{\pi} \left( \int_{\psi_-}^{\psi_+} w d\psi \right)^2, \quad (5.5)$$

where  $\psi_-$  and  $\psi_+$  are the minimum and maximum, respectively, of the the stream function. For this problem,

$$m^2 = \frac{1}{\pi} \int_0^1 (1 - r^2)^2 d\psi - \frac{1}{\pi} \left( \int_0^1 (1 - r^2)^2 d\psi \right)^2.$$

Letting  $d\psi = 2\pi r dr$ , ie the arc-length of a streamline times a differential radius amount, transforms the integral into an area integral

$$m^2 = 2 \int_0^1 (1 - r^2)^2 r dr - 1/4.$$

This evaluates to  $m^2 = 1/12$ , accounting for the behavior observed in the example above. This kind of mixing behavior is well-known in straight pipes.

### 5.3 $\lambda$ -dependent anomalous mixing

In this intermediate time mixing regime, we observe deviations from the  $1/\sqrt{12}$  slope observed above. A graph of  $\sigma$  versus  $t$  for various values of  $\lambda$  (see Figure 5.2) demonstrates that there is a relationship between  $\lambda$  and the deviation of Anomalous II from Anomalous I. Notice first that for large  $\lambda$ , there is little difference between Anomalous I and Anomalous II. If we examine the Poincaré

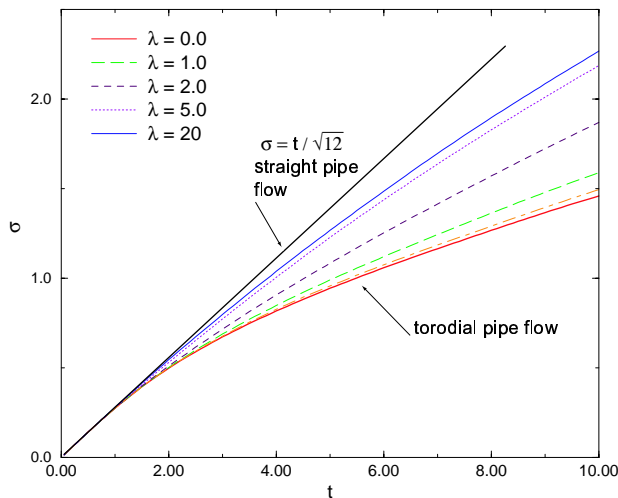


Figure 5.2: Plotting  $\sigma$  versus  $t$  for various values of  $\lambda$  reveals that the slope in the Anomalous II regime as well as the transition time between regimes depends of  $\lambda$ .

map streamlines in (3.11), we see that for large enough values of  $\lambda$ , the stream function has only  $r$  dependence and only models the rotation of the binormal that occurs in our helical coordinate system. Thus, for large  $\lambda$ , the pipe geometry is asymptotic to a straight pipe.

We examine two phenomena here: the dependence of  $t_t$  on  $\lambda$  and the dependence of the slope of Anomalous II on  $\lambda$ . Experimentally we obtain the relationship shown in Figure (5.3) between  $t_t$  and  $\lambda$ . Transition time  $t_t$  was determined by the first minimum in the second derivative. Since the transition from Anomalous I to Anomalous II is a transition between two linear pieces, we expect to see a second derivative plot that is zero except where nonlinear behavior occurs. Decreasing  $\lambda$  decreases the transition time. Figure (5.4) shows the relationship between the slope,  $m_\lambda$ , and  $\lambda$ . Increasing  $\lambda$  increases  $m_\lambda$ , implying that the cross-sectional mixing is slowing the longitudinal mixing.

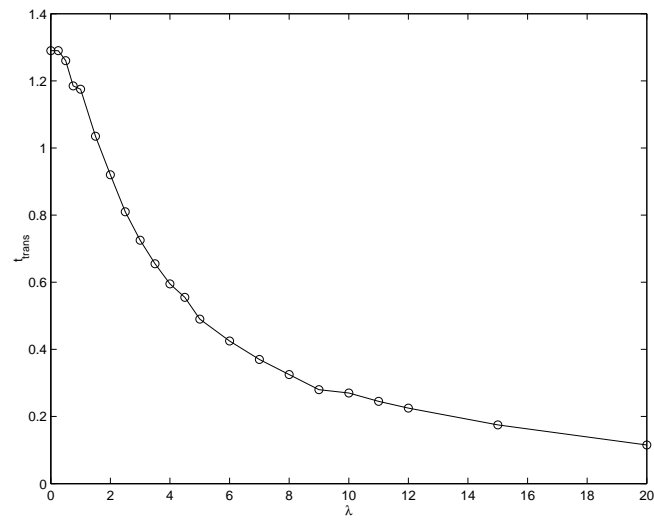


Figure 5.3: The transition time  $t_t$  from the Anomalous I to the Anomalous II regime depends on  $\lambda$  as shown above.

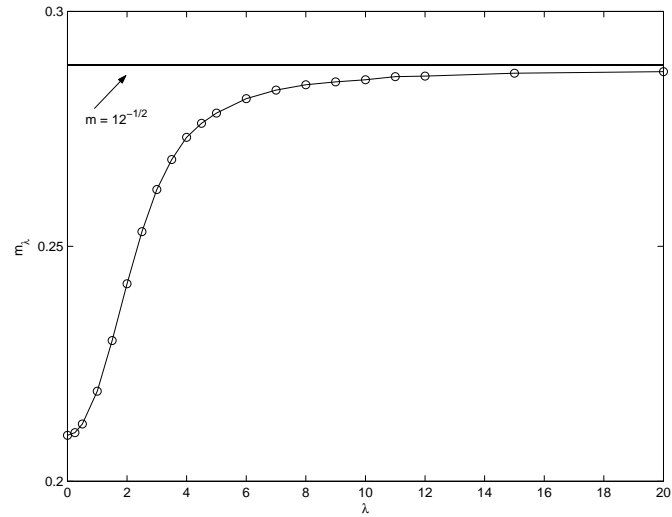


Figure 5.4: The Anomalous II slope  $m_\lambda$  has a direct relationship with  $\lambda$ . Large values of  $\lambda$  represent pipes that are nearly straight.

### 5.4 Taylor Dispersion dependence on torsion

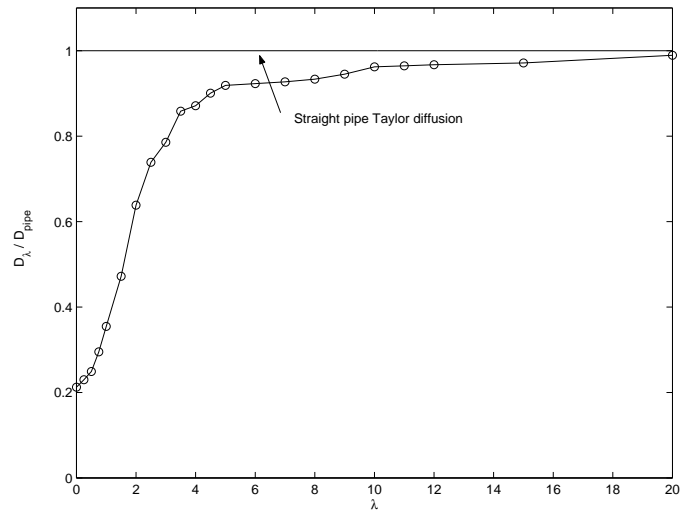


Figure 5.5: The Taylor diffusion constant  $D_{eff}$  shrinks as  $\lambda$  shrinks, implying that toroidal pipes mix slower at large  $t$ .

For  $t > 1/D$  we observe a Taylor Dispersion regime. The  $D_{eff}$  is larger for larger  $\lambda$ . Figure (5.5) shows this relationship. Since  $D_{eff}$  is proportional to  $1/D$ , we wish to find  $k = k(\lambda)$  such that  $D_{eff} = k/D$ . From the literature, it is known that for straight pipes ( $\lambda \gg 1$ ),  $k = 1/48$  [8], and for toroidal pipes ( $\lambda = 0$ ),  $k$  is smaller. Our observed values fall within this range.

## Chapter 6

### Conclusion

This thesis explored the effects of helical geometry on fluid mixing. We derived the standard ODE model of flow in toroidal pipes (Dean flow) in Chapter 2. By changing coordinates and demonstrating that torsion was a second order effect in the asymptotic expansion, we extended Dean flow to cover helical pipes. In Chapter 3, we found a stream function for the helical flow based on the toroidal flow function. With these equations, we constructed a numerical Monte Carlo simulation to measure mixing in Chapter 4. Errors in this computation were examined based on splitting apart the advective and diffusive process in the governing equations and on the stability of the ODE integrator.

#### **6.1 Results**

From this simulation, we observed in Chapter 5 four different scaling regimes of the longitudinal mixing, two of which were dependent on the geometry parameter  $\lambda$ . For very short times ( $t < D$ ), we observed a diffusive regime, where the effects of advection were not yet felt locally and  $\sigma \approx \sqrt{Dt}$ . For  $t < t_t$  (where  $t_t$  is the turnover time of the helical equations), we observe a ballistic or “anomalous” regime characteristic of straight-pipe mixing with a slope  $m = \sqrt{1/12}$ . For  $t_t < t < 1/D$ , a second anomalous ballistic regime occurs, where the slope  $m$  is a function of  $\lambda$ . Finally, for  $t \gg 1/D$ , we observe Taylor diffusion, where the effective diffusion constant,  $D_{eff}$ , depends on  $\lambda$ . Analysis showed that the slope of the second anomalous regime and the value

of  $D_{eff}$  are larger when  $\lambda$  is larger. Note that a very large  $\lambda$  value corresponds to a nearly straight pipe.

## 6.2 Future work

While this thesis has investigated the anomalous mixing regimes thoroughly, the Taylor regime deserves a more careful study. The relationship between the Taylor diffusion constant  $k$  and  $\lambda$  still needs to be established. This problem will require exploring the parameter space in both  $\lambda$  and  $D$ . However, for large  $\lambda$  and small  $D$ , this becomes very difficult to compute, as small timesteps are needed to resolve the fast coordinate rotation and long times are needed to observe Taylor Diffusion.

Using the method outlined in Section 5.2, one could extend the analysis to describe the Anomalous II mixing regime. In this case, the  $s$ -velocity would be a function of streamline and would be tricky to calculate, but the integration to find  $m$  would be straightforward.

The extension to pipes where  $\lambda$  is a function of  $s$  would be another good area of study. It is known (Germano [4]) that torsion can be a function of arc length without causing a first order change in the flow equations. Some restraint on curvature's relationship could suppress first-order variations from taking  $\kappa = \kappa(s)$ .

Physically, allowing particles near the boundary to escape with some small probability would change this problem from a mixing simulation to a heat-exchange simulation. Temperature could be measured by summing the number of "heat particles" contained in a given region and averaging over space. Since heat exchange depends more on mixing in the cross-section than longitudinally, the mixing properties of nearly toroidal helices could provide a no-moving-parts efficient heat exchange system.

## Bibliography

- [1] S.A. Berger and L. Talbot. Flow in curved pipes. *Ann. Rev. Fluid Mech.*, 15:461–512, 1983.
- [2] W.R. Dean. Note on the motion of a fluid in a curved pipe. *Phil. Mag*, 4:208–223, 1927.
- [3] M. Germano. On the effect of torsion on a helical pipe flow. *J. Fluid Mech.*, 125:1–8, 1981.
- [4] M. Germano. The dean equations extened to a helical pipe flow. *J. Fluid Mech.*, 203:289–305, 1987.
- [5] Scott W. Jones, Oran M. Thomas, and Hassan Aref. Chaotic advection by laminar flow in a twisted pipe. *J. Fluid Mech.*, 209:335–357, 1989.
- [6] Marco Latini. Mixing in curved pipes. Undergratuante thesis, Harvey Mudd College, 2001.
- [7] Marco Latini and Andrew J. Bernoff. Transient anomalous diffusion in poiseuille flow. *J. Fluid Mech.*, 2001.
- [8] M.J. Lighthill. Initial development of diffusion in poiseuille flow. *J. Inst. Maths Applics*, 2:97–108, 1966.
- [9] Joseph F. Lingevitch and Andrew J. Bernoff. Advection of a passive scalar by a vortex couple in the small-diffusion limit. *J. Fluid Mech.*, 270:219–249, 1994.

- [10] G.I. Taylor. Dispersion of soluble matter in solvent flowing slowly through a tube. *Proc. R. Soc. Lond. A*, 219:186–203, 1953.
- [11] A.J. Ward-Smith. *Internal fluid flow: the fluid dynamics of flow in pipes and ducts*, pages 248–255. Oxford University Press, 1980.
- [12] W.R. Young and Scott Jones. Shear dispersion. *Phys. Fluids A*, 3:1087–1101, 1991.